International Journal of Environmental Sciences
Vol. xx No. x (2025)
Copyright@ Academic Science Publications and Distributions
http://www.theaspd.com/ijes.php

SYNTHESIS AND CHARACTERIZATION OF CARBON QUANTUM DOTS (CQDS)/ZNO NANOCOMPOSITES: APPLICATION TO TEXTILES FOR EFFICIENT ORGANIC CONTAMINANTS AND PARTICULATE MATTER REMOVAL

Ihsanul Huda [1], Surachate Kalasin [*1],
Pantawan Sangnuang [2], Werasak Surareungchai [2]
[1] *Faculty of Science, Nanoscience & Nanotechnology Graduate Program, King Mongkut's University of Technology Thonburi (KMUTT), 10140, Bangkok, Thailand*
[2] *Pilot Plant Research and Development Laboratory, King Mongkut's University of Technology Thonburi, 10150 Bangkok, Thailand*
Email: ihsanulhuda326@gmail.com, surachate.kal@kmutt.ac.th, pantawan.san@kmutt.ac.th, werasak.sur@kmutt.ac.th
**Corresponding Author:* surachate.kal@kmutt.ac.th

Received: xxx
Revised: xxx
Accepted: xxx

Abstract
Particulate matter (PM) and organic contaminants present a significant health problem due to their small size and complicated composition. Herein, we proposed carbon quantum dots (CQDs)/ZnO nanocomposite coated on cheap and widely available fibrous materials, which are textiles (silk, cotton, and polyester) that have the ability to remove PM and organic contaminants. The CQDs/ZnO nanocomposites were fabricated using a facile hydrothermal approach from CQDs that were obtained from biowaste tamarind shells. Coated textiles with CQDs/ZnO nanocomposites were tested with PM and photocatalytic activity using methylene blue (MB) as a model organic contaminant. The presence of CQDs on CQDs/ZnO nanocomposites can improve the filtration efficiency of textiles by ~8% of silk, ~22% of cotton, and ~38% of polyester. The result showed that cotton-CQDs/ZnO have the best removal efficiency (88.5% for PM10 and 88% for PM2.5) and demonstrated excellent washable reusability. In addition, textile-CQDs/ZnO exhibited excellent photocatalytic activity with 7.1, 7.4, and 9.1 times better than uncoated silk, cotton, and polyester, respectively, under UV light. The unique properties of CQDs, such as their high surface area, rich functional groups, and charge separation, combined with the adsorption capability and physical properties of ZnO, can contribute to PM capture and organic contaminants removal effectively. Thus, due to several properties and compatibility with various types of textiles, the CQDs/ZnO nanocomposites can be easily integrated into existing air filtration systems to remove air pollution

Keywords: *Particulate Matter, Carbon Quantum Dots, Zinc Oxide, Nanocomposites, Textiles*

1. Introduction

Air is contaminated with fine dust particles such as particulate matter (PM). Particulate matter 10 and 2.5 (PM10 and PM2.5) is composed of various chemical substances, such as nitrate, sulfate, silicate, carbon, and ammonium, which refers to a particle size below 10 and 2.5 μm [1]. PM pollution is hazardous for the community because these small particles can penetrate the bronchi and human lungs [2]. PM is produced by vehicle exhaust, industrial activity, road dust, forest fires, and sand dust storms, and its

inhalation can occur in the home, workplace, and the ambient environment. With the complex composition and small size, removing and regulating PM remains a major challenge [3].

PM is accompanied by some harmful gaseous pollutants such as carbon monoxide (CO), nitrogen oxides (NO_x), Sulfur dioxide (SO_2), and organic contaminants such as volatile organic compounds (VOCs)[4]. VOCs are one of the most dangerous air pollutants, usually present indoors and outdoors. VOCs are mostly vaporized easily at room temperature, and their concentration is higher than other pollutants in the indoor air. Interactions between VOCs species and other pollutants can also lead to adverse human health outcomes, such as respiratory effects and neurological symptoms [5,6]. Therefore, the development of multifunctional materials that can simultaneously remove organic contaminants and PM is crucial to study.

Until now, there have been two types of air filter materials that are used for PM filtration, porous and fibrous filters [2]. Filters can be composed of various materials, such as textiles or fabrics [7], oxides [8], metals [9,10], carbon-based materials [11,12], and advanced materials [13,14]. Textile is one of the cheap and widely available fibrous textile materials. It is flexible, has good mechanical properties, and has low airflow resistance [15]. Those properties can be used as a filter to remove air pollution. Moreover, the rich potential binding sites in textiles make it a promising substrate for incorporating nanomaterials to improve or add their properties [15].

Several studies have successfully incorporated ZnO into textiles to remove PM [16] and organic contaminants [17,18]. The presence of ZnO in the enhancement of filtration performance was attributed to increasing surface potential and surface roughness of fiber, allowing the capture of PM [19]. ZnO also shows promising effects in photocatalysis to remove organic contaminants due to its wide bandgap, high electron mobility, and great transparency in the ultraviolet-visible range [20]. To improve adsorption range, surface charge, functional groups, and charge separation for removing particulate matter and organic contaminants application, incorporating other materials such as carbon quantum dots (CQDs) to produce nanocomposites is a promising technique [21–23].

CQDs have a small size of 1–10 nm and provide several advantages, including being easy to produce, having great chemical stability, having strong electron conductivity, and being biocompatible [24]. Due to its simplicity, cost-effectiveness, scalability, and environmental-friendliness, the hydrothermal approach is a promising method for producing mono-dispersed CQDs [25,26]. An effective and promising alternative material for producing CQDs is cheap and sustainable sources of raw materials, such as biowaste [27]. Tamarind shells are brittle and are primarily generated as a biowaste by-product of the tamarind pulp industry [28]. The high carbon content of tamarind shells has been used for several applications [29–31]. Moreover, tamarind shells are affordable in price and generally have abundant local availability. Therefore, tamarind shell has a promising carbon source to produce CQDs and fabricate CQDs/ZnO nanocomposites.

Although there are several reports on the CQDs/ZnO nanocomposites application, simultaneous efforts should be made to explore a new application of CQDs/ZnO nanocomposites, especially for organic contaminants and PM removal applications. Moreover, investigating the interactions between CQDs, ZnO, and air pollutants can provide insights into adsorption, photocatalytic activity, and air purification processes. Therefore, further investigations in the field of CQDs and ZnO as air filters may provide potential directions for the development of more efficient, sustainable, and cost-effective air filtration technologies.

Herein, we utilized tamarind shells as a carbon source to produce CQDs, while CQDs/ZnO nanocomposites were produced from a green synthesis technique. CQDs/ZnO nanocomposites were coated on different types of textiles (silk, cotton, polyester) and evaluated for their ability to remove PM and organic contaminants. The mechanism of CQDs/ZnO nanocomposite coated on textiles and the effect of CQDs/ZnO nanocomposite for PM and organic contaminants removal were also studied in this work.

2. Method

2.1 Materials and reagents

The textiles (polyester, cotton, silk), tamarind fruits (Tamarindus indica), and incense sticks (diameter: 0.3 cm, length: 2.6 cm, weight: 1.45 g) were purchased from a local market. Zinc acetate dihydrate ($Zn(CH_3CO_2)_2 \cdot 2H_2O$), sodium hydroxide (NaOH), acetone (C_3H_6O), and methylene blue ($C_{16}H_{18}ClN_3S$) were purchased from Merck company (Darmstadt, Germany).

2.2 Synthesis of CQDs

The tamarind shells were separated from the tamarind fruits and broken into medium-sized. Then, a medium-sized tamarind shell was dried and reduced using a mortar to obtain powder. The 3.75 g tamarind shell powder was dispersed in 75 ml deionized water and the mixture was heated in Teflon-lined stainless steel autoclave at 180°C for 12 h. The dispersion obtained was filtered through a Whatman grade No. 1 filter paper, followed by a 0.2 µm membrane filter. The brown-colored solution of as-prepared CQDs was stored at 4°C for further use.

2.3 Synthesis of ZnO and CQDs/ZnO nanocomposite

2.4 g of zinc acetate dehydrate and CQDs solution (40 ml) were mixed by using a magnetic stirrer at room temperature. Then, NaOH 0.5M was added dropwise until the pH reached 10. The solution mixture was placed in a 100 mL stainless steel autoclave at 80°C for 3 h. The precipitate was separated by centrifugation at 8,000 rpm for 10 min. The precipitate was washed several times with deionized water to remove impurities. Finally, the white-brown powder of CQDs/ZnO nanocomposites was obtained by drying the precipitate at 60°C overnight, sealed, and stored at 4°C for further use. For ZnO synthesis was conducted with 40 ml of DI water without CQDs solution under same procedure.

2.4 Fabrication of ZnO and CQDs/ZnO nanocomposites coated on textiles

For the pretreatment of textiles, all the samples (silk, cotton, polyester) having a size of 5 cm x 5 cm were washed with detergent and water. Then, the textiles were immersed in 1M of NaOH solution at 80°C for 30 min after being cleaned with acetone, followed by rinsing with water and drying at 55°C for 24 h. Textiles coated with ZnO and CQDs/ZnO nanocomposites were fabricated using a dip-coating approach. The dried textiles were immersed in ZnO and CQDs/ZnO nanocomposite solution under an ultrasonic bath at 50°C for 40 min and dried at 55°C overnight. The ZnO and CQDs/ZnO solution was prepared by diluting 1 g of CQDs/ZnO powder in 100 ml of DI water. The Immersion-drying process was undertaken three times in succession. The textiles were heated at 200°C for 30 min to remove weakly attached particles and rinsed with DI water followed by drying at 55°C for 24 h

2.5 PM Measurement

The PM test in this experiment setup was illustrated in Figure 1. Burning incense served as the source of the PM particles used in this experiment, which flowed into a glass box (40 x 12 x 12 cm). On the surface of the fan (5.64 watt, CHB12012DS-A model SuperRed, China), sample was positioned in the center of the box (flow rate of air: 4.2 L/min and window size of filter: 4.5 x 4.5 cm). Before and after the PM passed through the sample, the PM concentration was measured using PM detectors (BR-8A model, detection range 0-999 µg/m^3, accuracy 0.001 µg/m^3, KKMOON, China) and recorded by digital camera (1.920 x 1.080 pixels x 30 fps) for 30 min. The high concentration of PM before filtration was used (PM2.5 average = 377 µg/m^3 and PM10 average = 441 µg/m^3). This experimental setup is to evaluate the performance of the filter under harsh working conditions. For PM detector calibration, the gravimetric method was applied [32]. The filtration efficiency (E_s) will be measured by using this equation [33,34]:

$$E_s\ (\%) = \frac{C1-C2}{C1}\ x\ 100$$

Where *C1* (mg/m^3) is the particle number concentration before treatment, and *C2* (mg/m^3) is the particle number concentration after treatment. The filtration efficiency is one of the key evaluation parameters for evaluating PM filters and is related to the material structure, thickness, porosity, and airflow velocity [33].

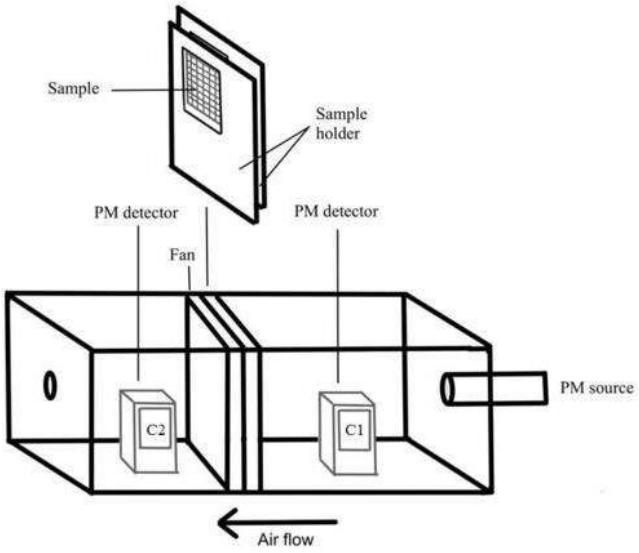

Figure 1. PM measurement setup

2.6 Photocatalytic activity test

Photocatalytic activity of the untreated and treated textiles was studied using methylene blue (MB) as the model organic compound under UV light illumination. Each sample was immersed in 10 mg/L of 40 ml MB solution with stirring. The absorbance of the remaining or degraded MB was then determined using UV-Vis spectroscopy with 500-700 nm wavelength. The photocatalytic efficiency was measured by observing absorbance of MB at 665 nm wavelength and calculated by using this equation:

$$\text{Photocatalytic efficiency (\%)} = \frac{C_0 - C_t}{C_0}\ x\ 100$$

Where C_0 is the initial concentration of MB, and C_t is the concentration of MB after 't minutes.

2.7 Characterization

The UV-Vis absorption was recorded using a NanoPhotometer N60 spectrophotometer (Implen) with wavescan mode (200-900 nm wavelength) and photoluminescence spectra of solutions in 96 well plate were recorded using a Cytation 5 (BioTek, Germany with Gen5 3.05 software) with wavescane mode (300 – 700 nm wavelength). Fourier transform infrared (FTIR) spectra was recorded (diamond prism with single bounce reflection) using an INVENIO R FTIR instrument (Bruker, USA) with attenuated total reflectance (ATR) measurement technique to observe the functional group of solid samples in 500-4000 cm^{-1} wavenumber (dimension of uncoated and coated textiles are 1 cm x 1 cm). X-ray powder diffraction (XRD) pattern of samples in powder was recorded by a Rigaku (SmartLab, Japan) diffractometer using Cu-Kα as the radiation source in 0-80 (2θ, degree). Dynamic light scattering (DLS) measurements were carried out by Malvern Zetasizer, UK to investigate the hydrodynamic size and zeta potential of samples in water solvent. The structure and morphology analysis of the CQDs, CQDs/ZnO nanocomposites, uncoated, and coated textiles were carried out by field emission scanning electron microscopy (FESEM) (FEI Nova Nanosem 450, USA). Elemental analysis was investigated by using Energy Dispersive X-ray spectroscopy (EDS) (Nano Xflash 6/3, Bruker, USA). CQDs and CQDs/ZnO were deposited on a silicon substrate for this measurement. The washed cotton-CQDs/ZnO were observed by scanning electron microscopy (SEM) Phenom Pharos (Thermo Scientific, USA) with 5 kV accelerating voltage.

Transmission electron microscope (TEM) was conducted with a 120 kV accelerating voltage (JEM-2100, JEOL, USA).

3. Result and Discussion

3.1 Characterization result of CQDs, ZnO, and CQDs/ZnO

The photoluminescence (PL) intensity of the prepared CQDs, ZnO, and CQDs/ZnO were investigated to know the excitation-emission properties (Figure 2). The CQDs solution is pale yellow under normal light and emits strong blue fluorescence under UV light (Figure 2a inset). The fluorescence intensity of the prepared CQDs was affected by excitation wavelength. When the excitation wavelength was increased from 320 to 420 nm, the emission peak became red-shifted from 420 nm to 500 nm. The emission intensity decreased as the excitation wavelength increased from 360 to 420 nm. This emission was mainly attributed to defect states and intrinsic defects of the CQDs [35]. The wavelength of the strongest emission peak of the CQDs was 440 nm, which belongs to blue–violet light. This indicates that the PL spectrum of our CQDs have excitation-dependent emission properties.

Moreover, due to CQDs having excitation at 360 nm, PL intensity of CQDs/ZnO and ZnO sample was also investigated under 360 nm excitation. ZnO sample showed the lowest emission compared CQDs/ZnO and CQDs. While the emission of the CQDs/ZnO nanocomposite has a lower PL intensity compared to the CQDs. This outcome is mostly the result of photo-excited electron and hole recombination being suppressed [36]. Emission at around 410 nm from CQDs/ZnO can be attributed to the near band-edge emission of ZnO [37] and emission at 440 nm occurred due to CQDs presence which showed the effective interaction between ZnO and CQDs [38]. Thus, the presence of CQDs on the surface of ZnO can extend the light absorption range due to the CQDs' ability to absorb a broader spectrum of light. This broader absorption range allows for increased utilization of light for the degradation of organic contaminants in photocatalytic activity study.

UV-visible spectroscopy was used to measure the absorption of CQDs, ZnO, and CQDs/ZnO nanocomposites. The CQDs samples exhibit a typical absorption peak at 280 nm. CQDs/ZnO nanocomposites sample showed a peak at 363 nm, while a peak at 362 nm was appeared from ZnO sample due to typical absorption of ZnO (Figure 2b). Based on the absorption data, A wide variety of energy bandgaps for CQDs (3.80 eV), ZnO (2.45 eV), and CQDs/ZnO nanocomposite (2.12 eV) were found (Figure 2c). CQDs/ZnO have the narrowest bandgap due to the ZnO semiconductor's current state [39]. The narrow band gap indicates that the photon energy is available to promote electrons from the valence band to the conduction band. The existence of a narrower band gap can widen the range of excitation wavelengths that can be absorbed, which facilitates the creation of reactive oxygen species (ROS) that can decompose air pollutants, thereby increasing photocatalytic performance [40].

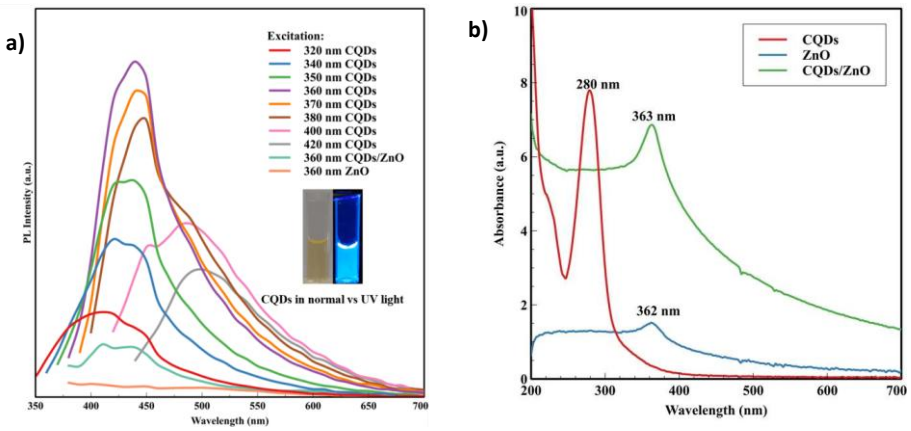

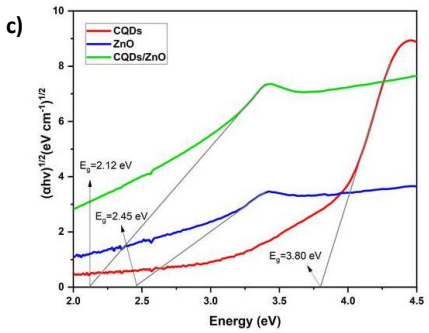

Figure 2. Optical properties of CQDs, ZnO, and CQDs/ZnO. (a) Emission from different excitation from 320 to 420 (inset: CQDs dispersed in water under normal light and UV light); (b) UV-Vis spectroscopy result; (c) Bandgap energy.

FTIR spectroscopy was used to analyze the chemical structure and functional group of the prepared samples (Figure 3a). For CQDs, the broad absorption band at 3300 cm−1 corresponds to O–H stretching vibrations. The bands at about 1400 cm-1 were associated with the bending vibration of C-N, whilst the bands at 1630 cm-1 were related to stretching vibrations of the C=C in the carboxyl group and amido group, the bands at 1140 cm-1 were attributed to C-H bonds. While in ZnO sample, showed O-H, C=C, and Zn-O bonds. Moreover, the CQDs/ZnO nanocomposite sample contained C-H and O-H bonds that appeared due to CQDs. The strong absorption bands around 615 cm-1 were attributed to the typical Zn-O bond absorption peak, and were also found in ZnO sample [41]. Based on this result, it was demonstrated that CQDs are loaded on ZnO to form CQDs/ZnO. CQDs possess a surface that is rich in functional groups that can serve as binding sites for ZnO nanoparticles, leading to the formation of chemical bonds and interactions between CQDs and ZnO.

XRD analysis was also used for CQDs, ZnO, and CQDs/ZnO samples (Figure 3b). CQDs sample showed two peaks at 2θ = 14° and 22°. The strong peak at 22° corresponds to (001) and (002) planes of graphite [42,43]. For ZnO and CQDs/ZnO sample showed that the diffraction peaks at 2θ = 31.74°, 34.42°, 36.28°, 47.64°, 56.62°, 62.80°, 66.24°, 67.92°, and 69.10° corresponded to the crystalline planes (100), (002), (101), (102), (110), (103), (200), (112), and (201) of the hexagonal ZnO wurtzite structure (JCPD36-1451). One peak from CQDs (001 planes) appeared in CQDs/ZnO samples, which indicated the presence of CQDs. The presence of a very small carbogenic core in CQDs is confirmed by the existence of a wider peak in the 2θ = 29 corresponding to (002) hkl plane in the sample [44]. The formation of small CQDs leads to the conclusion that a wider peak is implied. When the size of the crystallite was reduced, the XRD pattern peaks broadened. To know more the effect of CQDs in CQDs/ZnO sample, the peaks of CQDs between 2θ = 10° to 30° was observed (Figure 3c). It showed peaks from CQDs and had different intensities between CQDs/ZnO and ZnO samples towards CQDs region. Those phenomena may be ascribed to the interaction of small amounts CQDs and ZnO [39,45]. The data is in accordance with that reported on ZnO/CQDs prepared using different approaches [23,46]. Based on the functional groups and interaction between CQDs and ZnO, CQDs/ZnO showed a potential application for removing PM and organic contaminants.

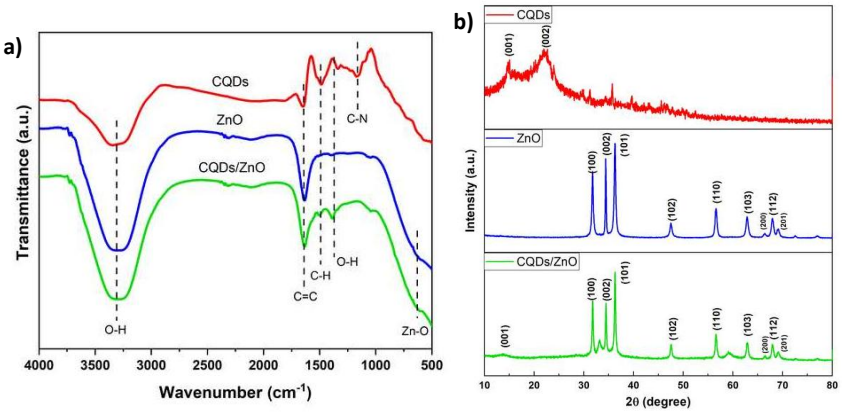

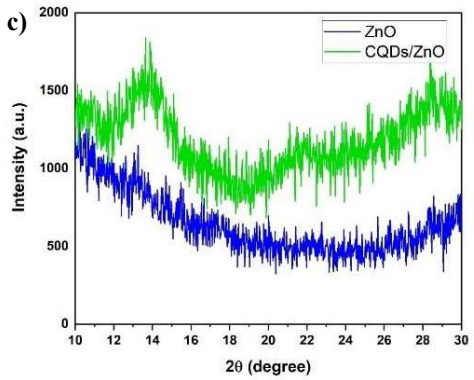

Figure 3. Characterization result of CQDs, ZnO, and CQDs/ZnO. (a) FTIR result; (b) XRD result; (c) XRD result at CQDs range (2θ = 10 – 30)

Zeta potential was conducted by using DLS to measure the surface charge of prepared sample. The negative surface charge (-30.7 mV) was shown in CQDs sample which indicated the CQDs have good stability, while ZnO has positive surface charge (16.1 mV). When CQDs and ZnO was combined to form nanocomposites, it showed negative surface charge (-18.0 mV) due to the presence CQDs on the surface of ZnO (Figure 4a). Based on this result, CQDs with surface charges (negative) can interact electrostatically with the oppositely charged surface of ZnO (positive), leading to attractive forces and binding between the materials. Furthermore, CQDs/ZnO may have a polar charge (negative surface charge from CQDs and positive surface charge from ZnO) that can generate electrostatic interaction to capture the polar charge of the PM. On the other hand, the polar surface charge also affects interaction with VOCs structure towards adsorption and electrostatic interaction.

The hydrodynamic size of ZnO and CQDs/ZnO were also investigated by dynamic light scattering (DLS). ZnO has a hydrodynamic size of 297.5 nm while CQDs/ZnO nanocomposite has a bigger hydrodynamic size of 301.6 nm. This might be due to the presence of CQDs on ZnO surface (Figure 4b). In this section, the hydrodynamic size of CQDs was not presented due to the DLS machine having a limitation to detect samples with high fluorescence. The size characterization of CQDs/ZnO was also studied using FESEM. The exposed sample area of CQDs/ZnO had uniformly sized with an average size was 267.2 nm (Figure 4c). Since DLS and FESEM have a limitation to measure <10 nm or exact CQDs size, TEM was used to analyze the morphology and size distribution of prepared CQDs. As shown in Figure 4d, CQDs showed spherical shape and 2.769 nm of the average particle size. This result confirmed the successful synthesis of CQDs from biowaste tamarind shells. Thus, CQDs typically have a high surface area due to their small size. The increased surface area provides more opportunities for the CQDs to interact and bind to the surface of ZnO. As a result, a larger number of CQDs can be accommodated on the ZnO surface, leading to higher coverage and the potential for enhanced interactions. These binding interactions are crucial for achieving synergistic effects and enhanced properties in CQDs/ZnO nanocomposites for removing PM and organic contaminants applications.

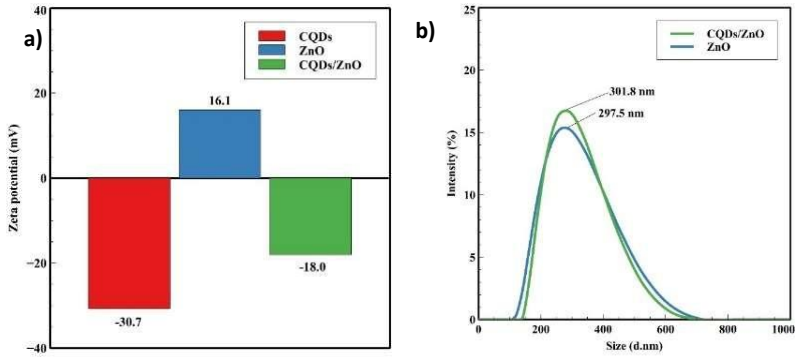

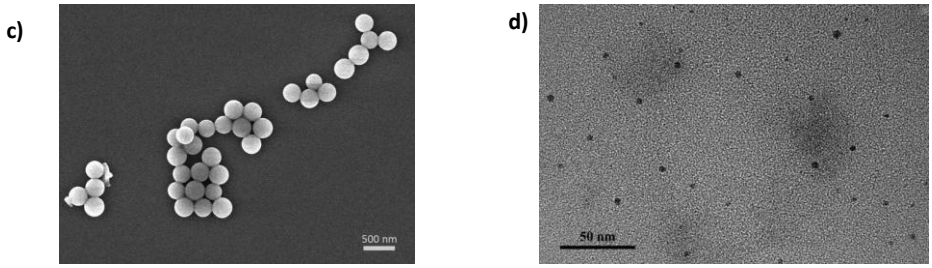

Figure 4. (a) Zeta potential result; (b) Hydrodynamic size result; (c) FESEM result of CQDs/ZnO; (d) TEM result of CQDs

3.2 Characterization result of coated textiles

The coated and uncoated samples were also analyzed by FTIR to investigate the interactions between textiles with ZnO and CQDs/ZnO nanocomposite (Figure 5). The XRD spectrum result of uncoated silk revealed three distinct peaks that were attributed to the C=O, C-O, and C=C bonds at 1711, 1098, and 714 cm^{-1}, respectively (Figure 5a). Strong peaks of uncoated cotton appeared at 1725, 1045, and 705 cm^{-1} due to the C=O, C-O-C, and C=C bonds (Figure 5b). For uncoated polyester, the C=O, C-O, and C=C bonds were responsible for the strong peaks at 1715, 1235, and 715 cm^{-1} (Figure 5c). After coating with ZnO and CQDs/ZnO nanocomposite, the additional peaks were identified at 500–552 cm^{-1} Due to the characteristic peak of the Zn-O bond from ZnO and CQDs/ZnO nanocomposite on the surface of textiles[47]. Surprisingly, in all textile-CQDs/ZnO samples, the peaks from 1800-800 cm^{-1} were found different from uncoated and coated textiles with ZnO. This might be the presence of CQDs in CQDs/ZnO samples toward coordination bond between functional groups in textiles and CQDs/ZnO through hydroxy or carboxylic groups.

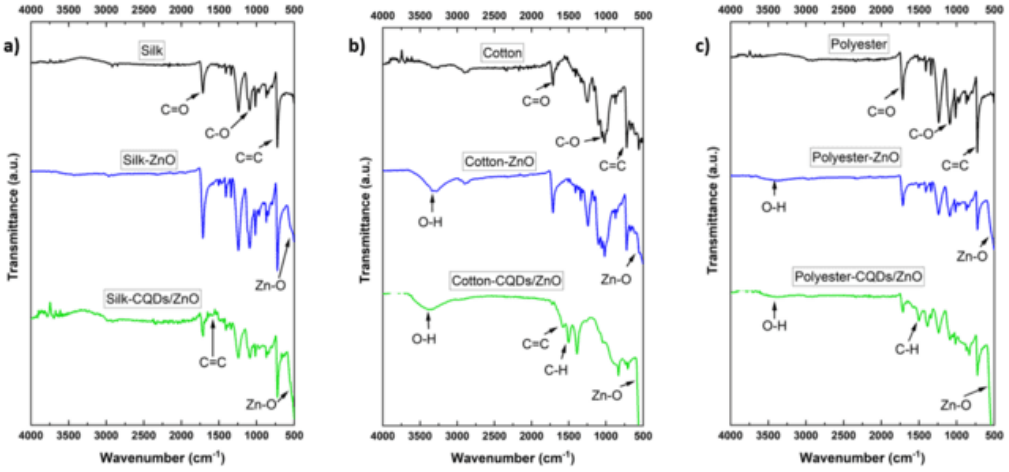

Figure 5. FTIR result of uncoated and coated textiles. (a) Silk; (b) Cotton; (c) Polyester

XRD result provided additional evidence of the CQDs/ZnO nanocomposite's attachment to the textiles. As shown in Figure 6, uncoated textiles (silk, cotton, and polyester) had an XRD pattern with three strong peaks at 17°, 22°, and 25° that were attributed to (110), (002), and (101), respectively, which were characteristic of the crystal structure of textiles [48]. The three peaks in the XRD pattern of the uncoated textiles were similar in positions and intensities to those of textile-ZnO and textile-CQDs/ZnO. This demonstrated that coating had no impact on the crystal structure of the textile [49]. All textile-ZnO and textile-CQDs/ZnO samples had nine additional peaks that are similar with the XRD results of the ZnO and CQDs/ZnO nanocomposites. It indicated that the textiles were successfully coated with ZnO and CQDs/ZnO.

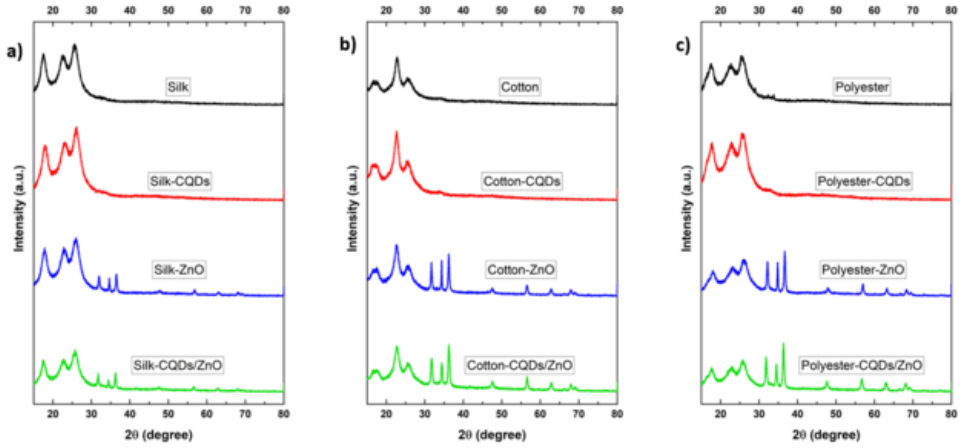

Figure 6. XRD result of uncoated and coated textiles. (a) Silk; (b) Cotton; (c) Polyester

Uncoated and coated textiles with CQDs/ZnO nanocomposite were also studied using FESEM EDS to know the surface morphology and elemental present of the produced samples. Based on the previous characterization results, textile-CQDs/ZnO showed the promising result for PM and organic contaminants removal study, therefore, the FESEM-EDS characterization of textiles-ZnO were not analyzed. Uncoated silk, cotton, and polyester have smooth surfaces Figure 7a-c whereas textiles coated with CQDs/ZnO have rough surfaces Figure 7d-f. In this case, elemental analysis of prepared samples was identified using EDS mapping (Figure 8). The presence of carbon (C) together with zinc (Zn) and oxygen (O) indicates the presence of CQDs with ZnO. These results were in line with previous characterization results and further confirmed the successful incorporation of CQDs/ZnO nanocomposite on the textile surface for PM and organic contaminants studies.

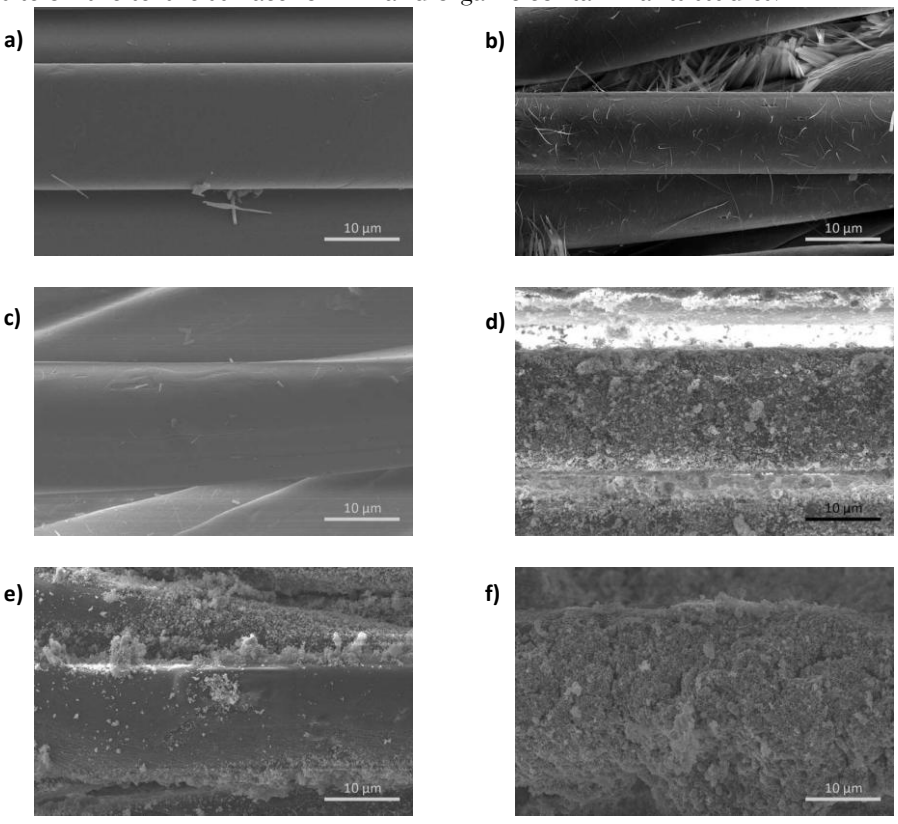

Figure 7. FESEM result. (a) silk; (b) cotton; (c) polyester; (d) silk-CQDs/ZnO; (e) cotton-CQDs/ZnO; (f) polyseter-CQDs/ZnO

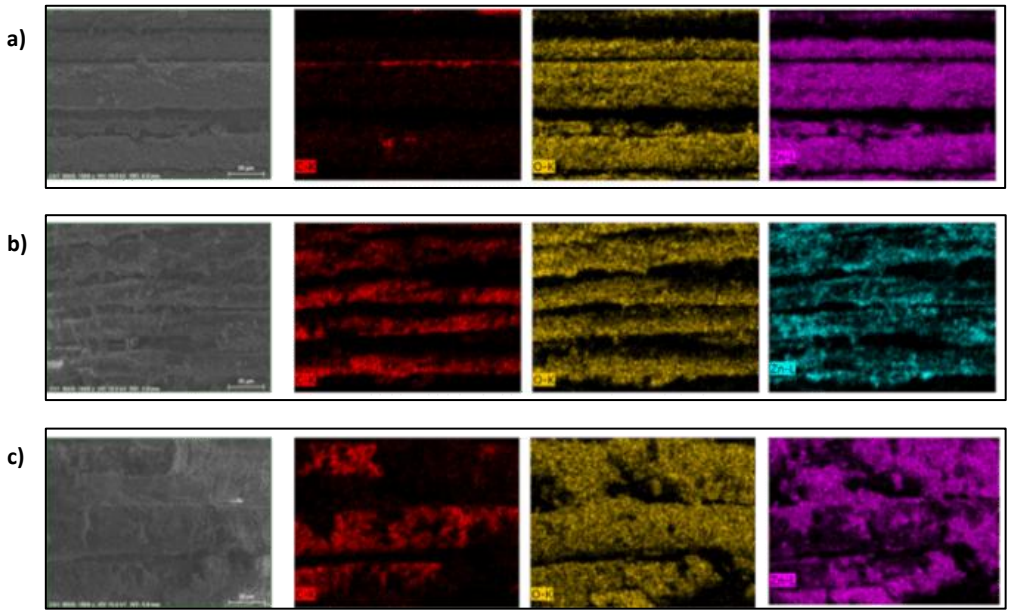

Figure 8. EDS mapping result. (a) silk-CQDs/ZnO; (b) cotton-CQDs/ZnO; and (c) polyester-CQDs/ZnO

3.3 CQDs/ZnO coated on textiles mechanism

CQDs/ZnO nanocomposites were successfully loaded on different kinds of textiles (silk, cotton, polyester), which was confirmed by FTIR, XRD, and FESEM EDS. The deposition of CQDs/ZnO nanocomposites on textile surfaces can occur through one of the two possible mechanisms. First, the coordination bond between functional groups in textiles and CQDs/ZnO (O-H, C=O, and C-O) through hydroxy or carboxylic groups. The second would be that textiles can act as chelating ligands, enabling metal ions (Zn) to interact and create Zn-O-C or Zn-OOC hybrid bonds via Zn-OH reactions from CQDs/ZnO nanocomposites and HO-C or HOOC from textiles [14,50,51].

3.4 PM measurement result

In PM test experiment, the performance of the filter under harsh working conditions was evaluated with detailed information in. A slight increase in filtration efficiency was found in coated silk with the presence of ZnO, and CQDs/ZnO (Figure 9a). This might be due to the small amount of ZnO, and CQDs/ZnO deposited on silk. However, the coated cotton and polyester showed a significant increase in filtration efficiency, which coated polyester showed more significant increase in filtration efficiency (Figure 9b-c). This also indicated that the higher amount of ZnO, and CQDs/ZnO was deposited on polyester rather than cotton and silk. Overall, the textiles-CQDs/ZnO showed the highest filtration efficiency compared with uncoated textiles and textiles-ZnO. Thus, the amount of ZnO and CQDs/ZnO deposited on textiles give a significant influence for filtration efficiency. After the PM test, FESEM images of coated textiles coated with CQDs/ZnO revealed that no significant structural change had occurred (Figure 9d-f) which also indicated its ability to withstand the PM.

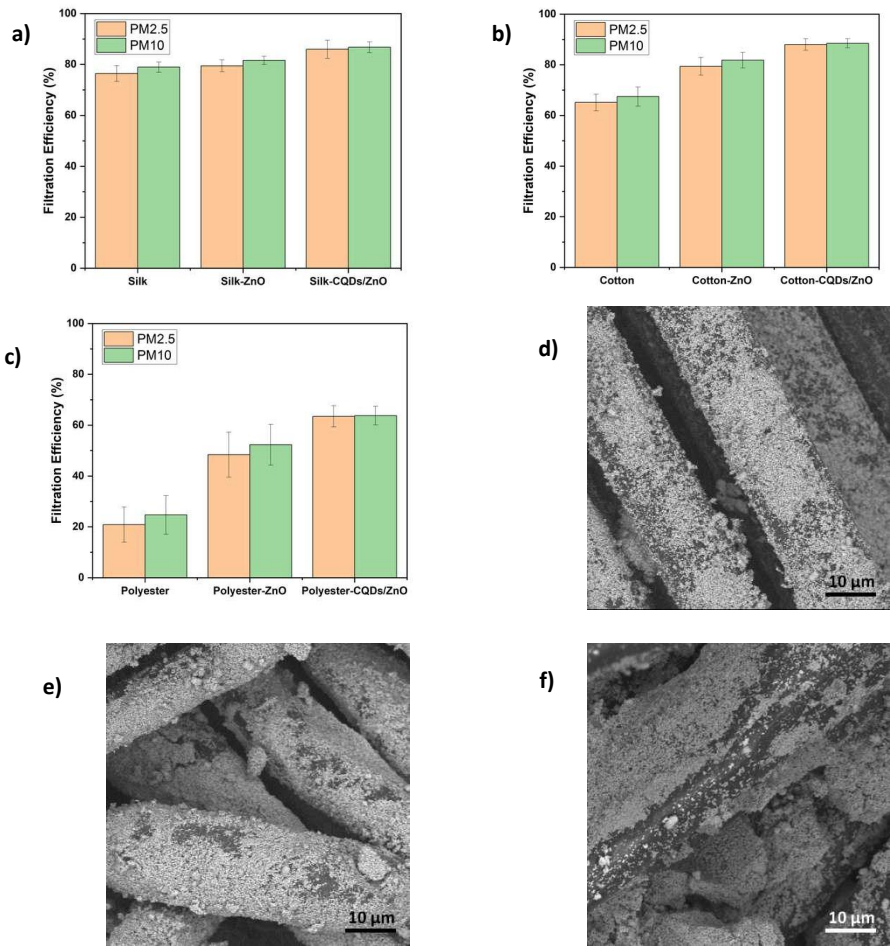

Figure 9. PM measurement result of uncoated and coated textiles. (a) Silk; (b) Cotton; (c) Polyester. FESEM result after PM test of (d) silk-CQDs/ZnO, (e) cotton-CQDs/ZnO, and (f) polyester-CQDs/ZnO

Since the cotton-CQDs/ZnO showed the best result of filtration efficiency (88.5% for PM10 and 88% for PM2.5), the performances of studied uncoated and cotton-CQDs/ZnO, were also checked for a wide range of initial concentrations of PM2.5 and PM10 (Figure 10a-b). Importantly, the removal efficiency of all the uncoated and coated did not depend noticeably on the initial concentrations of PM2.5 and PM10, which is supported by the good linear relationship between before and after PM concentrations with the minimum R^2 of 0.958. Moreover, the filtration efficiency of cotton-CQDs/ZnO to remove PM2.5 and PM10 was three times than uncoated cotton as calculated from slopes. Furthermore, the cotton-CQDs/ZnO was selected to investigate the recycling efficiency as an example by washing with water and then drying at room temperature. The cycling PM filtration efficiency of cotton-CQDs/ZnO was maintained at high levels (>87% for PM10 and >85% for PM2.5) (Figure 10c). No significant structural change was also observed in the FESEM picture of washed cotton-CQDs/ZnO which means the good washability and reusability (Figure 10d).

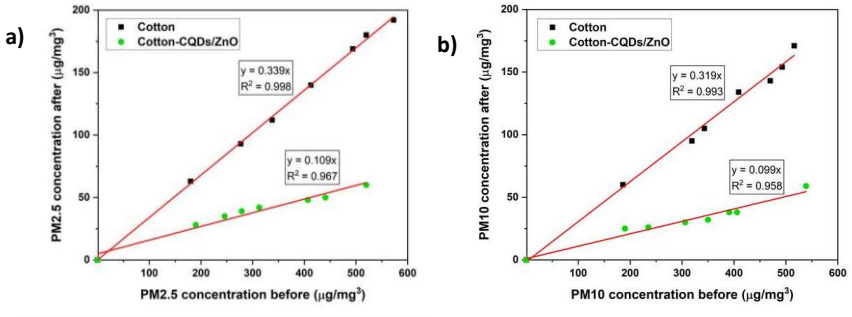

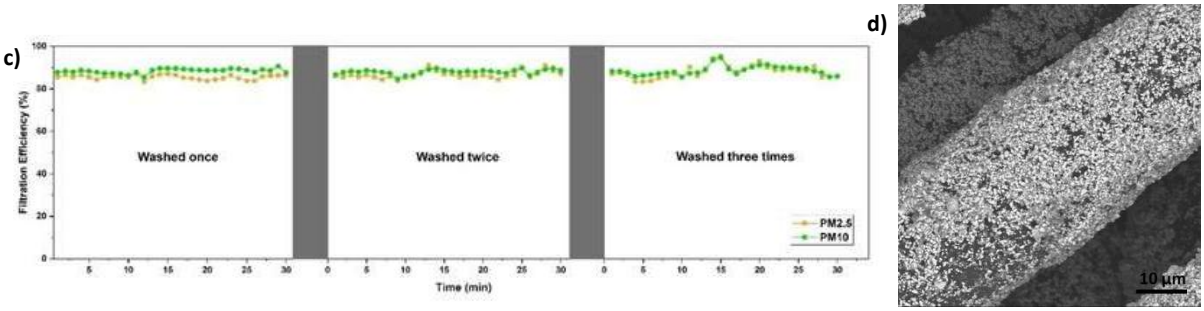

Figure 10. Concentration of PM before and after filtration; (a) PM2.5; (b) PM10. (c) PM test result of washed cotton-CQDs/ZnO; (d) FESEM result of washed cotton-CQDs/ZnO after PM test

3.5 PM removal mechanism of textile-CQDs/ZnO

The fact that all textile-CQDs/ZnO outperformed all uncoated textile and textile-ZnO in terms of filtration efficiency, Figure 11 indicates that CQDs/ZnO nanocomposites are crucial to the PM filtering process. The textile provides air filters with a macroporous structure and good structural stability. While, the presence of CQDs in textile-CQD/ZnO significantly enhances the filter surface area, which is advantageous for capturing PM [2]. Furthermore, the presence of CQDs/ZnO on the textile results in fibers with a high degree of surface roughness, which significantly increases the frictional force between PM [52,53].

In addition, the CQDs in CQDs/ZnO nanocomposites increase the surface charge and provide more functional groups that can attract PM through electrostatic interactions. Several functional groups with high polarity may be found on the surface of PM, including C-O, C-N, -NO3, and –SO3H [54]. When electric charge carrier particles are applied to a material, PM in the airflow is electrostatically adsorbed [52], and unipolar or bipolarly charged particles and fibers attract each other. Thus, surface modification by CQDs/ZnO can also improve electrical binding, which allows PM to be electrostatically trapped [55].

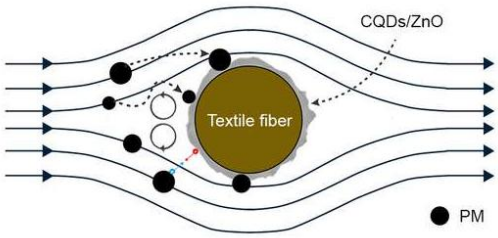

Figure 11. PM removal mechanism of textile-CQDs/ZnO

3.6 Photocatalytic activity result

The photocatalytic activity of textile, textile-ZnO, and textile-CQDs/ZnO samples was evaluated by examining the amount of degradation of MB as model organic contaminants under UV irradiation. First, MB solutions containing samples were stirred for 60 min in the dark to achieve the adsorption–desorption equilibrium, respectively. The solution of samples was collected every 20 min for 100 min after the light was turned on. Samples were then analyzed using a UV–Vis spectrophotometer at 665 nm, which is the maximum absorption wavelength of MB. Figure 12a-c shows the decrease in the absorbance of the sample solution towards MB as a function of time. A slight decrease in absorbance was observed in the dark period (-60 min to 0 min) due to dye adsorption into the sample. However, when the light was turned on, the sample showed a gradual decrease in absorption over time which was caused by the decrease in MB concentration due to the photocatalytic reaction of the sample. The greatest decrease in absorbance was shown in variations of textiles coated with CQDs/ZnO (Silk-CQDs/ZnO, Cotton-

CQDs/ZnO, and Polyester-CQDs/ZnO) compared to uncoated textiles and textiles coated with ZnO (Silk-ZnO, Cotton-ZnO, and Polyester-ZnO). Furthermore, the photocatalytic efficiency was calculated based on absorbance data. Figure 12d shows the photocatalytic efficiency of uncoated and coated silk. Uncoated silk achieved 19% of photocatalytic activity, whereas silk-ZnO and silk-CQDs/ZnO achieved 49% and 72%. The 29%, 64%, and 88% of photocatalytic efficiency was achieved by uncoated cotton, cotton-ZnO, and cotton-CQDs/ZnO (Figure 12e). In uncoated and coated polyester samples, polyester-CQDs/ZnO showed the highest photocatalytic efficiency (92%) than uncoated polyester (28%) and polyester-ZnO (67%) (Fig.11f). Overall, all samples of textiles coated with CQDs/ZnO showed the highest photocatalytic efficiency result.

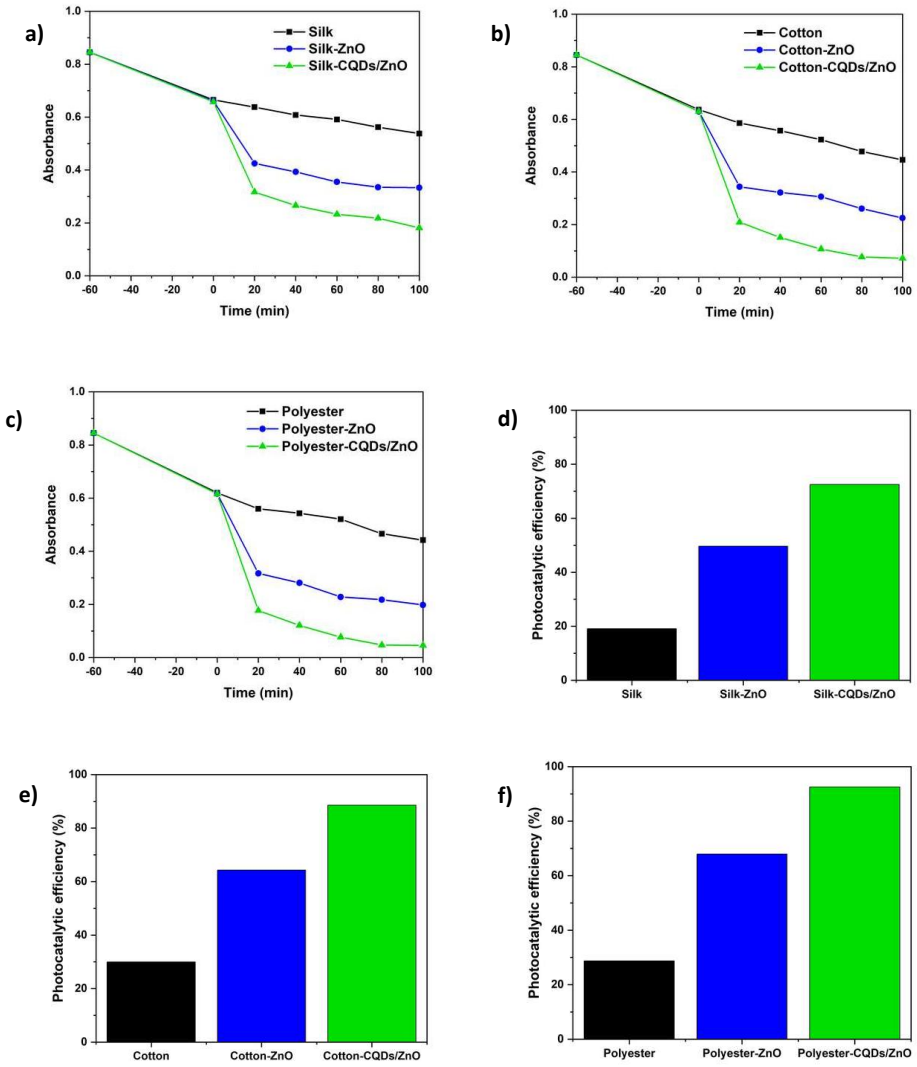

Figure 12. Absorbance of the sample solution towards MB, (a) Silk; (b) Cotton; (c) Polyester. Photocatalytic efficiency, (d) Silk; (e) Cotton; (f) Polyester.

In addition, the first-order rate equation was used to study the rate of photocatalytic activity by this equation:

$$-\ln (C_0/C_t) = Kt$$

where K is the first-order rate constant (min^{-1}), and t is the reaction time (min). As shown in Figure 13, (C_0/C_t) and $-\ln (C_0/C_t)$ were plotted against time. The K value indicates how fast the reaction occurs that were calculated from the slope of the linear fittings. Figure 13a shows that K for silk-CQDs/ZnO was 7.1 times higher than uncoated silk and 1.7 times higher than silk-ZnO. Also, in Figure 13b, for cotton-

CQDs/ZnO, the K value showed 0.0259 min^{-1}, which is 7.4 times higher than uncoated cotton and 2.2 times higher than cotton-ZnO. The K value of polyester-CQDs/ZnO also showed 9.1 times higher than uncoated polyester and 2.3 times higher than polyester-ZnO (Figure 13c). Based on these results, it has been demonstrated that and the synergistic combination of CQDs and ZnO is a good strategy for having a high photocatalytic performance.

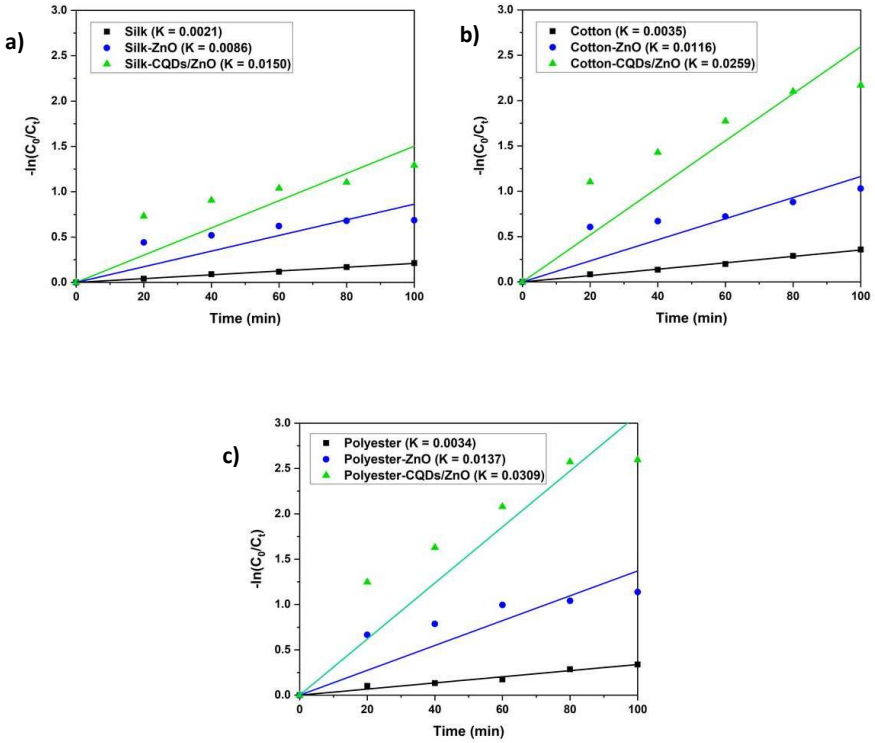

Figure 13. Degradation kinetics, (a) Silk; (b) Cotton; (c) Polyester

3.7 Textile-CQDs/ZnO Photocatalytic Activity Mechanism

The photocatalytic activity of materials for air filters is based on the principle that radiation of suitable wavelengths can be absorbed, which facilitates the creation of reactive oxygen species (ROS) that can decompose air pollutants [56]. Here, CQDs interact with adsorbed oxidants/reducers (usually O_2 and OH^-), they can excite ZnO to generate electron-hole pairs and react with them to produce significant amounts of active oxygen radicals, such as $^{\bullet}O_2^-$ and $^{\bullet}OH$. These radicals have strong oxidizing properties and can produce significant photodegradation of MB [57].

For the potential VOCs removal by photocatalytic method, the photoinduced electron-hole pair ($e^- h^+$) can undergo redox reactions at the surface of the photocatalyst and generate ROS[58]. Most forms of ROS react with adsorbed VOCs and transform them into partially oxidized states (intermediates) and completely oxidized states (CO_2 + H_2O) [59]. In addition, textiles have a function to adsorb organic contaminants by physical adsorption. Therefore, due to CQDs/ZnO showing good photocatalytic activity, it can be concluded that coated textile with CQDs/ZnO nanocomposite has the potential ability to remove other organic contaminants in the air.

4. Conclusion

The development of textiles-CQDs/ZnO as multifunctional materials that can simultaneously remove organic contaminants and PM was fabricated. CQDs were applied to ZnO to increase the adsorption range, surface charge, functional groups, and charge separation of ZnO, which restricts its application for removing particulate matter and organic contaminants. All coated textiles with CQDs/ZnO showed higher filtration and photocatalytic efficiency than coated textiles with ZnO and

uncoated textiles. The presence of functional groups in CQDs/ZnO can be deposited to various types of textiles to increase their ability for PM and organic contaminants removal application. The unique properties of CQDs combined with ZnO, contributed to effective PM capture and organic contaminants removal. The properties of CQDs/ZnO nanocomposites can be easily integrated into existing air filtration systems due to compatibility with various types of textiles. Further development efforts on real-world validation and addressing the environmental considerations of these materials should be focused. By addressing these perspectives, implementing CQDs/ZnO in air filters could become an effective and sustainable solution for improving air quality and reducing the impact of pollutants.

Author Contributions

I.H. wrote the manuscript with guidance from S.K. and W.S.; I.H., and P.S. carried out the experiments. S.K. and W.S. supervised the project, edited, and reviewed the manuscript.

Conflicts of interest

There are no conflicts to declare.

Acknowledgments

We thank King Mongkut's University of Technology Thonburi (KMUTT) for providing the Petchra Pra Jom Klao Master's Degree Scholarship to Mr. Ihsanul Huda. We also thank Nanoscience and Nanotechnology program, Faculty of Science KMUTT for facilitating the use of space and equipment during this research.

REFERENCES

[1] Liu, G., Xiao, M., Zhang, X., Gal, C., Chen, X., Liu, L., Pan, S., Wu, J., Tang, L., and Clements-Croome, D., 2017, "A Review of Air Filtration Technologies for Sustainable and Healthy Building Ventilation," Sustain Cities Soc, **32**, pp. 375–396. https://doi.org/https://doi.org/10.1016/j.scs.2017.04.011.

[2] Xiao, J., Liang, J., Zhang, C., Tao, Y., Ling, G.-W., and Yang, Q.-H., 2018, "Advanced Materials for Capturing Particulate Matter: Progress and Perspectives," Small Methods, **2**(7), p. 1800012. https://doi.org/https://doi.org/10.1002/smtd.201800012.

[3] Zhao, X., Li, Y., Hua, T., Jiang, P., Yin, X., Yu, J., and Ding, B., 2017, "Cleanable Air Filter Transferring Moisture and Effectively Capturing PM2.5," Small, **13**(11), p. 1603306. https://doi.org/https://doi.org/10.1002/smll.201603306.

[4] Su, J., Yang, G., Cheng, C., Huang, C., Xu, H., and Ke, Q., 2017, "Hierarchically Structured TiO2/PAN Nanofibrous Membranes for High-Efficiency Air Filtration and Toluene Degradation," J Colloid Interface Sci, **507**, pp. 386–396. https://doi.org/https://doi.org/10.1016/j.jcis.2017.07.104.

[5] Lerner, J. E. C., Kohajda, T., Aguilar, M. E., Massolo, L. A., Sánchez, E. Y., Porta, A. A., Opitz, P., Wichmann, G., Herbarth, O., and Mueller, A., 2014, "Improvement of Health Risk Factors after Reduction of VOC Concentrations in Industrial and Urban Areas," Environmental Science and Pollution Research, **21**(16), pp. 9676–9688. https://doi.org/10.1007/s11356-014-2904-x.

[6] Guo, H., Lee, S. C., Chan, L. Y., and Li, W. M., 2004, "Risk Assessment of Exposure to Volatile Organic Compounds in Different Indoor Environments," Environ Res, **94**(1), pp. 57–66. https://doi.org/https://doi.org/10.1016/S0013-9351(03)00035-5.

[7] Yoo, D. K., Woo, H. C., and Jhung, S. H., 2021, "Removal of Particulate Matters by Using Zeolitic Imidazolate Framework-8s (ZIF-8s) Coated onto Cotton: Effect of the Pore Size of ZIF-8s on Removal," ACS Appl Mater Interfaces, **13**(29), pp. 35214–35222. https://doi.org/10.1021/acsami.1c11796.

[8] Chuang, Y.-H., Hong, G.-B., and Chang, C.-T., 2014, "Study on Particulates and Volatile Organic Compounds Removal with TiO2 Nonwoven Filter Prepared by Electrospinning," J Air Waste Manage Assoc, **64**(6), pp. 738–742. https://doi.org/10.1080/10962247.2014.889614.

[9] Jeong, S., Cho, H., Han, S., Won, P., Lee, H., Hong, S., Yeo, J., Kwon, J., and Ko, S. H., 2017, "High Efficiency, Transparent, Reusable, and Active PM2.5 Filters by Hierarchical Ag Nanowire Percolation Network," Nano Lett, **17**(7), pp. 4339–4346. https://doi.org/10.1021/acs.nanolett.7b01404.

[10] Choi, D. Y., An, E. J., Jung, S. H., Song, D. K., Oh, Y. S., Lee, H. W., and Lee, H. M., 2018, "Al-Coated Conductive Fiber Filters for High-Efficiency Electrostatic Filtration: Effects of Electrical and Fiber Structural Properties," Sci Rep, **8**(1). https://doi.org/10.1038/s41598-018-23960-9.

[11] Hao, S.-W., Hsu, C.-H., Liu, Y.-G., and Chang, B. K., 2016, "Activated Carbon Derived from Hydrothermal Treatment of Sucrose and Its Air Filtration Application," RSC Adv, **6**(111), pp. 109950–109959. https://doi.org/10.1039/C6RA23958G.

[12] Li, P., Wang, C., Zhang, Y., and Wei, F., 2014, "Air Filtration in the Free Molecular Flow Regime: A Review of High-Efficiency Particulate Air Filters Based on Carbon Nanotubes," Small, **10**(22), pp. 4543–4561. https://doi.org/https://doi.org/10.1002/smll.201401553.

[13] Yoo, D. K., Woo, H. C., and Jhung, S. H., 2020, "Removal of Particulate Matters with Isostructural Zr-Based Metal–Organic Frameworks Coated on Cotton: Effect of Porosity of Coated MOFs on Removal," ACS Appl Mater Interfaces, **12**(30), pp. 34423–34431. https://doi.org/10.1021/acsami.0c08881.

[14] Zhang, K., Huo, Q., Zhou, Y.-Y., Wang, H.-H., Li, G.-P., Wang, Y.-W., and Wang, Y.-Y., 2019, "Textiles/Metal–Organic Frameworks Composites as Flexible Air Filters for Efficient Particulate Matter Removal," ACS Appl Mater Interfaces, **11**(19), pp. 17368–17374. https://doi.org/10.1021/acsami.9b01734.

[15] Emam, H. E., and Abdelhameed, R. M., 2017, "Anti-UV Radiation Textiles Designed by Embracing with Nano-MIL (Ti, In)–Metal Organic Framework," ACS Appl Mater Interfaces, **9**(33), pp. 28034–28045. https://doi.org/10.1021/acsami.7b07357.

[16] Zhong, Z., Xu, Z., Sheng, T., Yao, J., Xing, W., and Wang, Y., 2015, "Unusual Air Filters with Ultrahigh Efficiency and Antibacterial Functionality Enabled by ZnO Nanorods," ACS Appl Mater Interfaces, **7**(38), pp. 21538–21544. https://doi.org/10.1021/acsami.5b06810.

[17] Sudrajat, H., 2018, "Superior Photocatalytic Activity of Polyester Fabrics Coated with Zinc Oxide from Waste Hot Dipping Zinc," J Clean Prod, **172**, pp. 1722–1729. https://doi.org/https://doi.org/10.1016/j.jclepro.2017.12.024.

[18] Zhu, C., Shi, J., Xu, S., Ishimori, M., Sui, J., and Morikawa, H., 2017, "Design and Characterization of Self-Cleaning Cotton Fabrics Exploiting Zinc Oxide Nanoparticle-Triggered Photocatalytic Degradation," Cellulose, **24**(6), pp. 2657–2667. https://doi.org/10.1007/s10570-017-1289-7.

[19] Aamer, H., Heo, S., and Jo, Y.-M., 2021, "Characterization of Multifunctional PAN/ZnO Nanofibrous Composite Filter for Fine Dust Capture and Photocatalytic Activity," J Appl Polym Sci, **138**(26), p. 50607. https://doi.org/https://doi.org/10.1002/app.50607.

[20] Khalafi, T., Buazar, F., and Ghanemi, K., 2019, "Phycosynthesis and Enhanced Photocatalytic Activity of Zinc Oxide Nanoparticles Toward Organosulfur Pollutants," Sci Rep, **9**(1). https://doi.org/10.1038/s41598-019-43368-3.

[21] Velumani, A., Sengodan, P., Arumugam, P., Rajendran, R., Santhanam, S., and Palanisamy, M., 2020, "Carbon Quantum Dots Supported ZnO Sphere Based Photocatalyst for Dye Degradation Application," Current Applied Physics, **20**(10), pp. 1176–1184. https://doi.org/https://doi.org/10.1016/j.cap.2020.07.016.

[22] Liang, H., Tai, X., Du, Z., and Yin, Y., 2020, "Enhanced Photocatalytic Activity of ZnO Sensitized by Carbon Quantum Dots and Application in Phenol Wastewater," Opt Mater (Amst), **100**, p. 109674. https://doi.org/https://doi.org/10.1016/j.optmat.2020.109674.

[23] Bozetine, H., Wang, Q., Barras, A., Li, M., Hadjersi, T., Szunerits, S., and Boukherroub, R., 2016, "Green Chemistry Approach for the Synthesis of ZnO–Carbon Dots Nanocomposites with Good Photocatalytic Properties under Visible Light," J Colloid Interface Sci, **465**, pp. 286–294. https://doi.org/https://doi.org/10.1016/j.jcis.2015.12.001.

[24] Baker, S. N., and Baker, G. A., 2010, "Luminescent Carbon Nanodots: Emergent Nanolights," Angewandte Chemie International Edition, **49**(38), pp. 6726–6744. https://doi.org/https://doi.org/10.1002/anie.200906623.

[25] Liu, S., Tian, J., Wang, L., Zhang, Y., Qin, X., Luo, Y., Asiri, A. M., Al-Youbi, A. O., and Sun, X., 2012, "Hydrothermal Treatment of Grass: A Low-Cost, Green Route to Nitrogen-Doped,

Carbon-Rich, Photoluminescent Polymer Nanodots as an Effective Fluorescent Sensing Platform for Label-Free Detection of Cu(II) Ions," Advanced Materials, **24**(15), pp. 2037–2041. https://doi.org/https://doi.org/10.1002/adma.201200164.

[26] Titirici, M. M., Antonietti, M., and Baccile, N., 2008, "Hydrothermal Carbon from Biomass: A Comparison of the Local Structure from Poly- to Monosaccharides and Pentoses/Hexoses," Green Chemistry, **10**(11), pp. 1204–1212. https://doi.org/10.1039/B807009A.

[27] Prasannan, A., and Imae, T., 2013, "One-Pot Synthesis of Fluorescent Carbon Dots from Orange Waste Peels," Ind Eng Chem Res, **52**(44), pp. 15673–15678. https://doi.org/10.1021/ie402421s.

[28] Phani Kumar, N., Siva Kumar, N., and Krishnaiah, A., 2012, *DEFLUORIDATION OF WATER USING TAMARIND (TAMARINDUS INDICA) FRUIT COVER: KINETICS AND EQUILIBRIUM STUDIES*.

[29] Senthilkumar, S. T., Selvan, R. K., Melo, J. S., and Sanjeeviraja, C., 2013, "High Performance Solid-State Electric Double Layer Capacitor from Redox Mediated Gel Polymer Electrolyte and Renewable Tamarind Fruit Shell Derived Porous Carbon," ACS Appl Mater Interfaces, **5**(21), pp. 10541–10550. https://doi.org/10.1021/am402162b.

[30] Thirumal, V., Dhamodharan, K., Yuvakkumar, R., Ravi, G., Saravanakumar, B., Thambidurai, M., Dang, C., and Velauthapillai, D., 2021, "Cleaner Production of Tamarind Fruit Shell into Bio-Mass Derived Porous 3D-Activated Carbon Nanosheets by CVD Technique for Supercapacitor Applications," Chemosphere, **282**, p. 131033. https://doi.org/https://doi.org/10.1016/j.chemosphere.2021.131033.

[31] Muthukumaraswamy Rangaraj, V., Achazhiyath Edathil, A., Y. Kannangara, Y., Song, J.-K., Abu Haija, M., and Banat, F., 2019, "Tamarind Shell Derived N-Doped Carbon for Capacitive Deionization (CDI) Studies," Journal of Electroanalytical Chemistry, **848**, p. 113307. https://doi.org/https://doi.org/10.1016/j.jelechem.2019.113307.

[32] Shi, J., Chen, F., Cai, Y., Fan, S., Cai, J., Chen, R., Kan, H., Lu, Y., and Zhao, Z., 2017, "Validation of a Light-Scattering PM2.5 Sensor Monitor Based on the Long-Term Gravimetric Measurements in Field Tests," PLoS One, **12**(11), pp. e0185700-. [Online]. Available: https://doi.org/10.1371/journal.pone.0185700.

[33] Leung, W. W.-F., Hung, C.-H., and Yuen, P.-T., 2010, "Effect of Face Velocity, Nanofiber Packing Density and Thickness on Filtration Performance of Filters with Nanofibers Coated on a Substrate," Sep Purif Technol, **71**(1), pp. 30–37. https://doi.org/https://doi.org/10.1016/j.seppur.2009.10.017.

[34] Chen, C. Y., 1955, "Filtration of Aerosols By Fibrous Media," Chem Rev, **55**(3), pp. 595–623. https://doi.org/10.1021/cr50003a004.

[35] Velumani, A., Sengodan, P., Arumugam, P., Rajendran, R., Santhanam, S., and Palanisamy, M., 2020, "Carbon Quantum Dots Supported ZnO Sphere Based Photocatalyst for Dye Degradation Application," Current Applied Physics, **20**(10), pp. 1176–1184. https://doi.org/https://doi.org/10.1016/j.cap.2020.07.016.

[36] Azarang, M., Shuhaimi, A., Yousefi, R., and Sookhakian, M., 2014, "Effects of Graphene Oxide Concentration on Optical Properties of ZnO/RGO Nanocomposites and Their Application to Photocurrent Generation," J Appl Phys, **116**(8), p. 084307. https://doi.org/10.1063/1.4894141.

[37] Mukherjee, I., Cilamkoti, V., and Dutta, R. K., 2021, "Sunlight-Driven Photocatalytic Degradation of Ciprofloxacin by Carbon Dots Embedded in ZnO Nanostructures," ACS Appl Nano Mater, **4**(8), pp. 7686–7697. https://doi.org/10.1021/acsanm.1c00883.

[38] Guo, D.-Y., Shan, C.-X., Qu, S.-N., and Shen, D.-Z., 2014, "Highly Sensitive Ultraviolet Photodetectors Fabricated from ZnO Quantum Dots/Carbon Nanodots Hybrid Films," Sci Rep, **4**(1), p. 7469. https://doi.org/10.1038/srep07469.

[39] Yu, Z., Zhang, L., Wang, X., He, D., Suo, H., and Zhao, C., 2020, "Fabrication of ZnO/Carbon Quantum Dots Composite Sensor for Detecting No Gas," Sensors (Switzerland), **20**(17), pp. 1–11. https://doi.org/10.3390/s20174961.

[40] Ariga, H., Taniike, T., Morikawa, H., Tada, M., Min, B. K., Watanabe, K., Matsumoto, Y., Ikeda, S., Saiki, K., and Iwasawa, Y., 2009, "Surface-Mediated Visible-Light Photo-Oxidation on Pure TiO2(001)," J Am Chem Soc, **131**(41), pp. 14670–14672. https://doi.org/10.1021/ja9066805.

[41] Zhai, J., Wang, L., Wang, D., Lin, Y., He, D., and Xie, T., 2012, "UV-Illumination Room-Temperature Gas Sensing Activity of Carbon-Doped ZnO Microspheres," Sens Actuators B Chem, **161**(1), pp. 292–297. https://doi.org/https://doi.org/10.1016/j.snb.2011.10.034.

[42] Zhang, B., Liu, W., Wu, X., Zhu, J., Hu, W., El Jaouhari, A., and Liu, X., 2022, "Facile Preparation of Fluorescent Carbon Dots from Glutathione and l -Tryptophan for Sensitive and Selective Off/On Detection of Fe3+Ions in Serum and Their Bioimaging Application," ACS Omega, **7**(9), pp. 7853–7864. https://doi.org/10.1021/acsomega.1c06757.

[43] Wang, T., Wang, A., Wang, R., Liu, Z., Sun, Y., Shan, G., Chen, Y., and Liu, Y., 2019, "Carbon Dots with Molecular Fluorescence and Their Application as a 'Turn-off' Fluorescent Probe for Ferricyanide Detection," Sci Rep, **9**(1). https://doi.org/10.1038/s41598-019-47168-7.

[44] Krysmann, M. J., Kelarakis, A., Dallas, P., and Giannelis, E. P., 2012, "Formation Mechanism of Carbogenic Nanoparticles with Dual Photoluminescence Emission," J Am Chem Soc, **134**(2), pp. 747–750. https://doi.org/10.1021/ja204661r.

[45] Song, S., Wu, K., Wu, H., Guo, J., and Zhang, L., 2019, "Multi-Shelled ZnO Decorated with Nitrogen and Phosphorus Co-Doped Carbon Quantum Dots: Synthesis and Enhanced Photodegradation Activity of Methylene Blue in Aqueous Solutions," RSC Adv, **9**(13), pp. 7362–7374. https://doi.org/10.1039/c9ra00168a.

[46] Safardoust-Hojaghan, H., Salavati-Niasari, M., Amiri, O., Rashki, S., and Ashrafi, M., 2021, "Green Synthesis, Characterization and Antimicrobial Activity of Carbon Quantum Dots-Decorated ZnO Nanoparticles," Ceram Int, **47**(4), pp. 5187–5197. https://doi.org/https://doi.org/10.1016/j.ceramint.2020.10.097.

[47] Yedurkar, S., Maurya, C., and Mahanwar, P., 2016, "Biosynthesis of Zinc Oxide Nanoparticles Using Ixora Coccinea Leaf Extract—A Green Approach," Open Journal of Synthesis Theory and Applications, **05**(01), pp. 1–14. https://doi.org/10.4236/ojsta.2016.51001.

[48] Moafi, H. F., Shojaie, A. F., and Zanjanchi, M. A., 2011, "Photocatalytic Self-Cleaning Properties of Cellulosic Fibers Modified by Nano-Sized Zinc Oxide," Thin Solid Films, **519**(11), pp. 3641–3646. https://doi.org/https://doi.org/10.1016/j.tsf.2011.01.347.

[49] Shateri Khalil-Abad, M., Yazdanshenas, M. E., and Nateghi, M. R., 2009, "Effect of Cationization on Adsorption of Silver Nanoparticles on Cotton Surfaces and Its Antibacterial Activity," Cellulose, **16**(6), pp. 1147–1157. https://doi.org/10.1007/s10570-009-9351-8.

[50] Kim, H. H., Lee, Y., Lee, Y. J., Jeong, J., Yi, Y., Park, C., Yim, S.-Y., Angadi, B., Ko, K.-J., Kang, J.-W., and Choi, W. K., 2020, "Realization of Excitation Wavelength Independent Blue Emission of ZnO Quantum Dots with Intrinsic Defects," ACS Photonics, **7**(3), pp. 723–734. https://doi.org/10.1021/acsphotonics.9b01587.

[51] Emam, H. E., and Bechtold, T., 2015, "Cotton Fabrics with UV Blocking Properties through Metal Salts Deposition," Appl Surf Sci, **357**, pp. 1878–1889. https://doi.org/https://doi.org/10.1016/j.apsusc.2015.09.095.

[52] Wang, C.-S., 2001, "Electrostatic Forces in Fibrous Filters—a Review," Powder Technol, **118**(1), pp. 166–170. https://doi.org/https://doi.org/10.1016/S0032-5910(01)00307-2.

[53] Sambaer, W., Zatloukal, M., and Kimmer, D., 2012, "3D Air Filtration Modeling for Nanofiber Based Filters in the Ultrafine Particle Size Range," Chem Eng Sci, **82**, pp. 299–311. https://doi.org/https://doi.org/10.1016/j.ces.2012.07.031.

[54] Liu, C., Hsu, P.-C., Lee, H.-W., Ye, M., Zheng, G., Liu, N., Li, W., and Cui, Y., 2015, "Transparent Air Filter for High-Efficiency PM2.5 Capture," Nat Commun, **6**(1), p. 6205. https://doi.org/10.1038/ncomms7205.

[55] Kadam, V., Truong, Y. B., Easton, C., Mukherjee, S., Wang, L., Padhye, R., and Kyratzis, I. L., 2018, "Electrospun Polyacrylonitrile/β-Cyclodextrin Composite Membranes for Simultaneous Air Filtration and Adsorption of Volatile Organic Compounds," ACS Appl Nano Mater, **1**(8), pp. 4268–4277. https://doi.org/10.1021/acsanm.8b01056.

[56] Ren, H., Koshy, P., Chen, W.-F., Qi, S., and Sorrell, C. C., 2017, "Photocatalytic Materials and Technologies for Air Purification," J Hazard Mater, **325**, pp. 340–366. https://doi.org/https://doi.org/10.1016/j.jhazmat.2016.08.072.

[57] Zhao, L., Fan, L. Z., Zhou, M. Q., Guan, H., Qiao, S., Antonietti, M., and Titirici, M. M., 2010, "Nitrogen-Containing Hydrothermal Carbons with Superior Performance in Supercapacitors," Advanced Materials, **22**(45), pp. 5202–5206. https://doi.org/10.1002/adma.201002647.

[58] Rengifo-Herrera, J. A., Osorio-Vargas, P., and Pulgarin, C., 2022, "A Critical Review on N-Modified TiO2 Limits to Treat Chemical and Biological Contaminants in Water. Evidence That Enhanced Visible Light Absorption Does Not Lead to Higher Degradation Rates under Whole Solar Light," J Hazard Mater, **425**, p. 127979. https://doi.org/https://doi.org/10.1016/j.jhazmat.2021.127979.

[59] Li, Q., Zhang, S., Xia, W., Jiang, X., Huang, Z., Wu, X., Zhao, H., Yuan, C., Shen, H., and Jing, G., 2022, "Surface Design of G-C3N4 Quantum Dot-Decorated TiO2(001) to Enhance the Photodegradation of Indoor Formaldehyde by Experimental and Theoretical Investigation," Ecotoxicol Environ Saf, **234**, p. 113411. https://doi.org/https://doi.org/10.1016/j.ecoenv.2022.113411.